

Micro-Raman and Spreading Resistance Analysis on Beveled Implanted Germanium for Layer Transfer Applications

Rainey, P., Wasyluk, J., Perova, T., Hurley, R., Mitchell, N., McNeill, D., ... Armstrong, M. (2011). Micro-Raman and Spreading Resistance Analysis on Beveled Implanted Germanium for Layer Transfer Applications. *Electrochemical and Solid-State Letters*, 14(2)(2), H69-H72.

Published in:
Electrochemical and Solid-State Letters

Queen's University Belfast - Research Portal:
[Link to publication record in Queen's University Belfast Research Portal](#)

General rights

Copyright for the publications made accessible via the Queen's University Belfast Research Portal is retained by the author(s) and / or other copyright owners and it is a condition of accessing these publications that users recognise and abide by the legal requirements associated with these rights.

Take down policy

The Research Portal is Queen's institutional repository that provides access to Queen's research output. Every effort has been made to ensure that content in the Research Portal does not infringe any person's rights, or applicable UK laws. If you discover content in the Research Portal that you believe breaches copyright or violates any law, please contact openaccess@qub.ac.uk.



Micro-Raman and Spreading Resistance Analysis on Beveled Implanted Germanium for Layer Transfer Applications

Paul Rainey,^{a,*} Joanna Wasyluk,^b Tatiana Perova,^b Richard Hurley,^a
Neil Mitchell,^a David McNeill,^a Harold Gamble,^{a,*} and Mervyn Armstrong^a

^aSchool of Electrical Engineering and Computer Science, Northern Ireland Semiconductor Research Center, The Queen's University of Belfast, Belfast, BT9 5AH, Northern Ireland, United Kingdom

^bDepartment of Electronic and Electrical Engineering, University of Dublin, Trinity College, Dublin 2, Ireland

Raman and spreading resistance profiling have been used to analyze defects in germanium caused by hydrogen and helium implants, of typical fluences used in layer transfer applications. Beveling has been used to facilitate probing beyond the laser penetration depth. Results of Raman mapping along the projection area reveal that after post-implant annealing at 400°C, some crystal damage remains, while at 600°C, the crystal damage has been repaired. Helium implants create acceptor states beyond the projected range, and for both hydrogen and helium, 1×10^{16} acceptors/cm² remain after 600°C. These are thought to be vacancy-related point defect clusters.

© 2010 The Electrochemical Society. [DOI: 10.1149/1.3512999] All rights reserved.

Manuscript submitted August 26, 2010; revised manuscript received October 19, 2010. Published November 22, 2010.

With a view to fabrication of germanium-on-insulator substrates, based on the smart-cut process,¹ there is a need for a better understanding of the processes involved in defect evolution, caused by the hydrogen and helium implantation. Radiation damage is known to cause donor² and acceptor³ states in the bandgap of many semiconductors, through the formation of vacancies and interstitials, which, on annealing, interact with hydrogen, oxygen, or dopant atoms already present in the lattice structure. The published literature on the annealing behavior of the damaged and amorphous Ge after ion implantation is mainly limited to the heavy ions (e.g., Ga, As, Sb, In, P,⁴ Si, and Ge^{5,6}) at medium^{6,7} (10^{14} atoms/cm²) to low (10^{12} atoms/cm²) fluences. In all the cases the maximum annealing required for full recrystallization was 500°C for 30 min. Higher fluence heavy atom implantation results in more permanent structural defects, for example, the honeycomb structure.⁸ For implantations of lighter ions (H, He) into germanium, approaching the fluences required for the smart-cut process (10^{16} atoms/cm²), amorphization would not be expected. For example, Akatsu et al.⁹ reported Ge samples with H⁺ implants of dose 5×10^{15} – 7×10^{16} cm⁻² and implantation energy 15 and 80 keV. Samples were annealed in the temperature range between 280 and 400°C for 30–60 min, and transmission electron microscope (TEM) analysis revealed a high level of crystalline atomic order, with small platelet defects.

In the process of demonstrating a germanium-on-sapphire substrate,¹⁰ depletion mode action of p-channel MOS-FET transistors was observed on substrates fabricated by smart-cut and enhancement mode p-channel MOS-FET transistor, on substrates fabricated by grind and polish.¹¹ The possibility that the reduced performance of the devices on smart-cut substrates was related to implantation damage was the main motivation for this work. In recent years, several studies on electrically active defects related to hydrogen implantation in germanium have been performed using deep level transient spectroscopy (DLTS).¹² These generally involved implant doses at or below 10^{14} atoms/cm². It is therefore necessary to examine implant doses of several orders of magnitude higher than this, similar to those used in a smart-cut process. Carrier concentrations in silicon, germanium, and other semiconductors can be inferred from the resistivity profile obtained by the spreading resistance profiling (SRP). When used for determining doping structures in implanted semiconductors, it is important to anneal out the implantation damage, as the carrier concentration is calculated from a known reference mobility which, in practice, will be lower if crys-

tal damage is present. Therefore, in this work, Raman provides an additional analysis technique based on non-electrical mechanisms for a clearer interpretation of results.

Beveling is routinely used in the preparation of samples for SRP and can be useful in Raman spectroscopy analysis, where there is a requirement to probe deep into the materials or to probe multilayer or graded layer structures. Germanium has a much larger absorption coefficient compared to silicon, so the penetration depth of laser light at 633 nm in germanium is only ~ 80 nm, while, in many cases, the region of interest is much deeper than this. The depth profiling of composition and strain using Raman spectroscopy has been presented for beveled Si/Si_{1-x}Ge_x/Si structures in Refs. 13 and 14. Also, Raman analysis on GaAs beveled samples formed by chemical etching¹⁵ and polishing¹⁶ has been reported. This work reports for the first time, the Raman analysis on beveled, ion implanted germanium samples.

Experimental

Germanium substrates used in this study were n-type, Sb-doped and p-type, Ga-doped (100) wafers with varying resistivities (supplied by Umicore, Brussels, Belgium). The substrates were given an HF-based clean, then coated with a 300 nm thick layer of atmospheric pressure CVD SiO₂ from a silane precursor at 400°C. Densification of this layer was achieved by annealing in a nitrogen ambient at 600°C for 2 h. Substrates were implanted with various fluences of hydrogen (ranging from 3 to 6×10^{16} cm⁻²) or helium (3×10^{16} cm⁻²) with implantation energies (H⁺: 75 keV; He: 105 keV) selected for a projected range of around 350 nm into the germanium substrate (as listed in Table I). Substrates were aligned at a 7° angle and kept at close to ambient temperature throughout the implant. Samples were beveled at Solecon Laboratories, Nevada¹⁷ for SRP analysis. Spreading resistance profiles were used to calculate carrier concentrations, based on the assumption that the mobilities of the samples are similar to the calibration standards. It is noted that SRP on Ge is less precise than on Si,¹⁸ for various reasons (e.g., less controllable probe tip penetration and less complete calibration standards, etc.). Nonetheless, the profiles are believed to be a reliable tool in analyzing differences in the various implanted samples.¹⁹ The same samples were subsequently used for the Raman analysis.

Raman spectra were registered in backscattering geometry using a micro-Raman Renishaw (Gloucester, England) 1000 system equipped with a Leica (Wetzlar, Germany) microscope. An 1800 lines/mm grating was used for all measurements, providing a spectral resolution of ~ 1 cm⁻¹. The 633 nm line of a HeNe laser with a power of 5 mW was used as an excitation source. The laser spot was focused on the sample surface using a 50× objective with

* Electrochemical Society Active Member.

^z E-mail: p.rainey@ee.qub.ac.uk

Table I. Doping and implant concentration and temperature of annealing for beveled Ge samples implanted with hydrogen and helium. All samples beveled after annealing, except the second anneal given to sample 3.

Sample	Background Ge doping concentration (Sb)	Implant conditions	Annealing
1	p-type $6 \times 10^{16}/\text{cm}^3$	Hydrogen implantation	
		6×10^{16} atoms/cm ² , 150 keV	unannealed
2	n-type $5 \times 10^{14}/\text{cm}^3$	Hydrogen implantation	
		3×10^{16} atoms/cm ² , 150 keV	450°C/2 h
3	n-type $5 \times 10^{14}/\text{cm}^3$	Hydrogen implantation	
		3×10^{16} atoms/cm ² , 150 keV	450°C/2 h then beveled, then 600°C/2 h
4	n-type $2 \times 10^{15}/\text{cm}^3$	Helium implantation	
		3×10^{16} atoms/cm ² , 105 keV	400°C/2 h
5	n-type $2 \times 10^{15}/\text{cm}^3$	Helium implantation	
		3×10^{16} atoms/cm ² , 105 keV	300°C/4 h then 600°C/2 h

a short-focus working distance. Line mapping measurements were performed at a distance along the beveling surface ranging from 0 to $\sim 400 \mu\text{m}$ with a step size of few micrometers, where zero corresponds to the starting point of the measurements (see Fig. 1). At each step increment, the Raman spectra were recorded and from each spectra, the full width at half maximum (fwhm) of Ge-Ge Raman peak was plotted to form the linewidth maps. The Ge-Ge Raman peaks were fitted using a mixture of Gaussian and Lorentzian functions. With the knowledge of the bevel angle for each sample, it was possible to convert the lateral distance between mea-

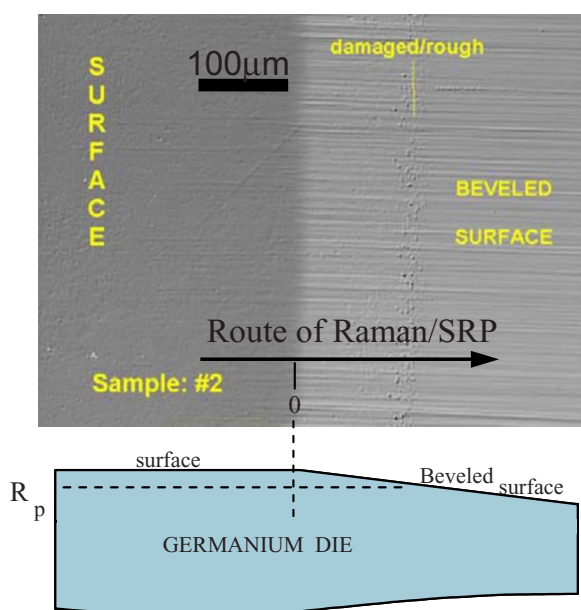


Figure 1. (Color online) Plan view optical microscopy image of Ge sample (with schematic cross section) implanted with 3×10^{16} atoms/cm² hydrogen dose and annealed at 450°C. The arrow indicates the direction and distance of the Raman line mapping.

surements into a vertical depth increment, and then superimpose the Raman data on the top of the carrier concentration versus depth plots (see Fig. 2).

Results and Discussion

Figure 1 shows an optical microscope image of a beveled Ge sample implanted with 3×10^{16} atoms/cm² hydrogen dose and annealed at 450°C, with structural damage clearly visible. This dose of 3×10^{16} atoms/cm² is slightly below the threshold of blistering for germanium because this is beneficial for analysis. Both SRP and Raman analysis would be detrimentally affected by the roughening caused by blisters. Beveling reveals that some defects and cavities form at the projected range due to the clustering of molecular hydrogen, but these are not large enough to be visible at the surface.

Raman spectra measured at the projection range for different Ge samples exhibit the Ge-Ge longitudinal optical phonon peak at $\sim 300 \text{cm}^{-1}$. When an implanted sample is annealed at high temperatures, the linewidth of the Ge-Ge peak returns to the value of high crystalline quality Ge. In preliminary trials, the structural defects caused by hydrogen implant were annealed out at 600°C in nitrogen atmosphere to yield a fully recovered structure, as measured by Raman. However, SRP on the same sample revealed a region of p-type acceptor states present at the projected range. Therefore, an extensive comparison of SRP and Raman has been undertaken.

For sample 1, a p-type Ge sample implanted with 6×10^{16} atoms/cm² of H⁺, without any subsequent anneals, SRP shows a high resistivity region running from the surface to the projected range. For the same sample, in Fig. 2a the carrier concentration derived from resistivity and Raman linewidth map are plotted. Raman shows a 7cm^{-1} fwhm peak, corresponding to the projected range. The lack of annealing for this sample hides the presence of acceptor states, as follows. The resistivity ρ along the bevel is a function of the majority carrier concentration, N , $\rho = 1/(Nq\mu)$, where μ is the majority carrier mobility and q is $1.6 \times 10^{19} \text{C}$. However, as mentioned in the introduction, defects that impair crystal quality can cause a reduction of mobility and therefore an increase in resistivity. The higher background concentration in sample 1 also shows more clearly the drop in the mobility caused by unannealed implant damage, stopping around $0.7 \mu\text{m}$ deep.

In Fig. 2b, the depth profiles of the Raman fwhm linewidths and carrier concentration are presented for sample 2 implanted with 3×10^{16} atoms/cm² and annealed to 450°C. This is a dose slightly below the threshold of blistering for germanium. Note the carrier-type change from n to p—this is consistent with the depletion mode action observed in p-MOS transistors.¹¹ Hydrogen in germanium is known to cause activation of otherwise inactive impurities.²⁰ For example, H-C and H-Si complexes are known to behave as shallow acceptors, and this is the most likely explanation for what is observed in Fig. 2b. The peak of $\sim 1 \times 10^{17} \text{cm}^{-3}$ acceptors and the maximum linewidth of Ge-Ge peak ($\sim 5.8 \text{cm}^{-1}$) are observed at the projected range of 350 nm. The projected range was confirmed by a SRIM (Ref. 21) simulation and by surface profile measurements on blistered samples and on layers which were transferred to handle substrates by smart-cut. The Raman fwhm peak of 5.8cm^{-1} detected at the projected range suggests some crystal disorder remaining after this anneal. For the 600°C annealed sample (see Fig. 2c), the SRP peak carrier concentration decreases about 1 order to 1×10^{16} acceptors/cm³, while the Raman linewidth profile is flat and corresponds to the high crystalline quality region of the unimplanted Ge wafer. There is a good correlation between the SRP and Raman at the deeper end of the implant (around $0.5 \mu\text{m}$ deep).

Helium has been used in layer transfer, in conjunction with hydrogen, to reduce the required dose for splitting.²² Helium implantation alone does not induce surface blistering in germanium, except at very high doses (several $\times 10^{17}$ atoms/cm²). Therefore, surface roughening due to blistering is not a problem with Raman or SRP. In Fig. 2d the Raman linewidth and carrier concentration are plotted

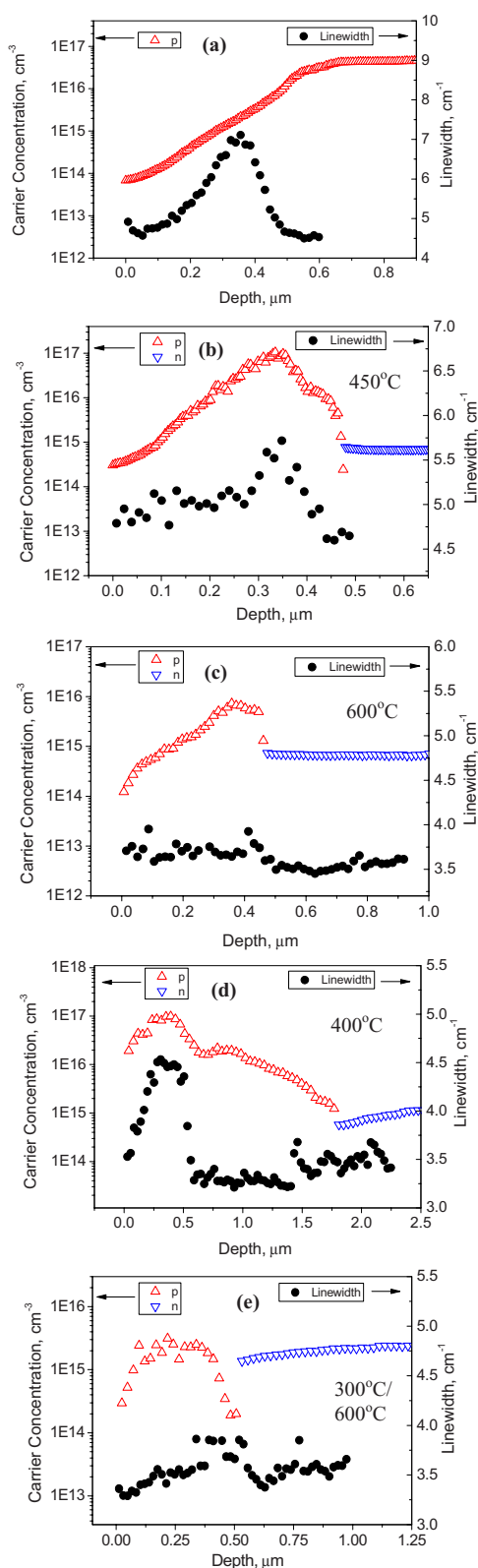


Figure 2. (Color online) Raman linewidth and carrier concentration derived from SRP vs depth into the sample for (a) 6×10^{16} atoms/cm² H⁺, (b) 3×10^{16} atoms/cm² H⁺ annealed to 450°C, and (c) to 600°C, (d) 3×10^{16} atoms/cm² He annealed to 400°C and (e) first anneal at 300°C then further annealing at 600°C.

versus depth for sample 4 implanted with 3×10^{16} atoms/cm² He and annealed at 400°C. SRP shows a peak of 1×10^{17} cm⁻³ ac-

ceptors at the projected range, and a second peak deeper into the substrate. The second peak is of special interest as this is much deeper than the simulated damage profile.²¹ For Raman, linewidth mapping on the 400°C sample shows a corresponding peak at the projected range, but the deeper feature does not appear. For silicon, it has been observed that helium implants produce a slight increase in self interstitials, which anneal out at moderate temperature.²³ It is also known that interstitial defects are more likely to occur beyond the projected range,²⁴ Alternatively, it has been proposed that the antimony–vacancy (Sb–V) complex is one of the main reasons for n to p conversion in Ge:Sb upon irradiation.²⁵ While Sb–V complexes could be expected to diffuse beyond the projected range via vacancy-mediated diffusion processes, in Ref. 25 the Sb–V complex was found to anneal out in the temperature range 140–180°C, much lower temperatures than the annealing received by samples 2–5. Also, a TEM study by David et al.²⁶ reported a similar finding for 5×10^{16} H⁺ in Ge; a highly damaged region around R_p and another, lesser damaged region, below this. The platelet defects in the deeper region were believed to be related to the strain distribution. Platelet defects are required for blisters to nucleate, but as mentioned above, for helium implants of 3×10^{16} , surface blistering does not occur. Therefore it is difficult to make a direct connection between the deeper features mentioned in Ref. 26 and those observed in Fig. 2d. In Fig. 2e the Raman linewidth map and carrier concentration are plotted for sample 5. The deeper feature observed in sample 4 disappears from the carrier concentration plot, while the peak at the projected range reduces in size, as in sample 3. From Fig. 2e, the flat Raman profile indicates the full damage recovery of the structure after 600°C annealing. Note that the background antimony concentration in this sample (2×10^{15} cm⁻²) is higher than in the sample shown in Fig. 2b and c (5×10^{14} cm⁻²). Comparing H⁺ and He implants after 600°C annealing, at first glance, the number of acceptors present appears lower for helium. However, as the measured carrier concentration is the sum of background Sb concentration and shallow acceptors, when the compensation by n-type Sb is deducted, the acceptor amounts are comparable. Another point of note when comparing H⁺ and He is that hydrogen passivation may reduce the prominence of these more stable features at R_p (and the deeper features) in the hydrogen implanted samples. The exact nature of these more stable defects is difficult to determine using SRP or Raman. Raman analysis indicates that the crystalline quality has been restored, which would suggest that they are point defects or complexes left behind after the recrystallization process.

Conclusions

A comparison and correlation of the electrical and structural properties of implant-related defects have been performed for “smart-cut-type” doses of hydrogen and helium in germanium. Using SRP, it has been found that for both ion species, a quantity of 1×10^{16} cm⁻² electrically active acceptors still remain after annealing at 600°C. Acceptors from the helium implantation appear significantly deeper than the projected range. Raman spectra show that at 600°C, the crystal damage has been repaired, which suggests that these remaining acceptor states are due to point defects or complexes.

Acknowledgments

The authors acknowledge the financial support of EPSRC (UK) in support of grant EP/E030130/1 and Royal society/RIA international joint project grant (2009–2011). J.W. would like to acknowledge the financial support of IRCSET Ireland, Postgraduate Award and ICGEE Ireland, Bursary Award.

Queen’s University, Belfast assisted in meeting the publication costs of this article.

References

1. M. Bruel, *Electron. Lett.*, **31**, 1201 (1995).
2. M. Cai, D. Qiao, L. S. Yu, S. S. Lau, C. P. Li, L. S. Hung, T. E. Haynes, K.

- Henttinen, I. Suni, V. M. C. Poon, et al., *J. Appl. Phys.*, **92**, 3388 (2002).
3. J. K. Lee, M. Nastasi, N. D. Theodore, A. Smalley, T. L. Alford, J. W. Mayer, M. Cai, and S. S. Lau, *J. Appl. Phys.*, **96**, 280 (2004).
 4. J. W. Mayer, L. Eriksson, S. T. Picraux, and J. A. Davies, *Can. J. Phys.*, **46**, 663 (1968).
 5. L. Csepregi, R. P. Kullen, J. W. Mayer, and T. W. Sigmon, *Solid State Commun.*, **21**, 1019 (1977).
 6. J. Slotte, M. Rummukainen, F. Tuomisto, V. P. Markevich, A. R. Peaker, C. Jeynes, and R. M. Gwilliam, *Phys. Rev. B*, **78**, 085202 (2008).
 7. S. Decoster and A. Vantomme, *J. Phys. D*, **42**, 165404 (2009).
 8. R. J. Kaiser, S. Koffel, P. Pichler, A. J. Bauer, B. Amon, A. Claverie, G. Benasayag, P. Scheiblin, L. Frey, and H. Ryssel, *Thin Solid Films*, **26**, 2323 (2010).
 9. T. Akatsu, K. K. Bourdelle, C. Richtarch, B. Faure, and F. Letertre, *Appl. Phys. Lett.*, **86**, 181910 (2005).
 10. H. S. Gamble, B. M. Armstrong, P. T. Baine, Y. H. Low, P. V. Rainey, Y. W. Low, D. W. McNeill, S. J. N. Mitchell, J. H. Montgomery, and F. H. Ruddell, *Mater. Sci. Semicond. Process.*, **11**, 195 (2008).
 11. P. T. Baine, H. S. Gamble, B. M. Armstrong, S. J. N. Mitchell, D. W. McNeill, P. V. Rainey, Y. H. Low, Y. W. Low, and D. Tantraviwat, in *Proceedings of IEEE International SOI Conference*, IEEE, p. 59 (2009).
 12. V. P. Markevich, L. Dobaczewski, K. B. Nielsen, V. V. Litvinov, A. N. Petukh, Yu. M. Pokotilo, N. V. Abrosimov, and A. R. Peaker, *Thin Solid Films*, **517**, 419 (2008).
 13. T. Mitani, S. Nakashima, H. Okumura, and A. Ogura, *J. Appl. Phys.*, **100**, 073511 (2006).
 14. R. M. B. Agaiby, S. H. Olsen, P. Dobrosz, H. Coulson, S. J. Bull, and A. G. O'Neill, *J. Appl. Phys.*, **104**, 013507 (2008).
 15. R. Srnanek, A. Vincze, J. Kovac, I. Gregora, D. S. Mc Phail, and V. Gottschalch, *Mater. Sci. Eng., B*, **91-92**, 87 (2002).
 16. A. Ito, M. Ichimura, A. Usami, T. Wada, and H. Kano, *J. Appl. Phys.*, **72**, 2531 (1992).
 17. <http://www.solecon.com>, last accessed November 14, 2010.
 18. T. Clarysse, P. Eyben, T. Janssens, I. Hoflijck, D. Vanhaeren, A. Satta, M. Meuris, W. Vandervorst, J. Bogdanowicz, and G. Raskin, *J. Vac. Sci. Technol. B*, **24**, 381 (2006).
 19. <http://www.solecon.com/bbs/messages/38.html>, last accessed November 13, 2010.
 20. J. Weber, M. Hiller, and E. V. Lavrov, *Mater. Sci. Semicond. Process.*, **9**, 564 (2006).
 21. <http://www.srim.org>, last accessed November 15, 2010.
 22. R. E. Hurley, H. Wadsworth, J. H. Montgomery, and H. S. Gamble, *Vacuum*, **83**, S29 (2009).
 23. G. F. Cerofolini, F. Corni, S. Frabboni, C. Nobili, G. Ottaviani, and R. Tonini, *Mater. Sci. Eng. R.*, **27**, 1 (2000).
 24. J. W. Mayer, L. Eriksson, and J. A. Davies, *Ion Implantation in Semiconductors, Silicon and Germanium*, Academic Press, New York (1970).
 25. V. P. Markevich, A. R. Peaker, V. V. Litvinov, V. V. Emtsev, and L. I. Murin, *J. Appl. Phys.*, **95**, 4078 (2004).
 26. M. L. David, F. Pailloux, D. Babonneau, M. Drouet, J. F. Barbot, E. Simoen, and C. Claeys, *J. Appl. Phys.*, **102**, 096101 (2007).